^{89}Zr-Immuno-PET: Toward a Noninvasive Clinical Tool to Measure Target Engagement of Therapeutic Antibodies In Vivo

Yvonne W.S. Jauw[1,2], Joseph A. O'Donoghue[3], Josée M. Zijlstra[1], Otto S. Hoekstra[2], C. Willemien Menke-van der Houven van Oordt[4], Franck Morschhauser[5], Jorge A. Carrasquillo[6,7], Sonja Zweegman[1], Neeta Pandit-Taskar[6,7], Adriaan A. Lammertsma[2], Guus. A.M.S. van Dongen[2], Ronald Boellaard[2], Wolfgang A. Weber[6,7], and Marc C. Huisman[2]

[1]Department of Hematology, Cancer Center Amsterdam, Amsterdam UMC, Vrije Universiteit Amsterdam, Amsterdam, The Netherlands; [2]Department of Radiology and Nuclear Medicine, Cancer Center Amsterdam, Amsterdam UMC, Vrije Universiteit Amsterdam, Amsterdam, The Netherlands; [3]Department of Medical Physics, Memorial Sloan Kettering Cancer Center, New York, New York; [4]Department of Medical Oncology, Cancer Center Amsterdam, Amsterdam UMC, Vrije Universiteit Amsterdam, Amsterdam, The Netherlands; [5]EA7365-GRITA-Groupe de Recherche sur les forms Injectables et les Technologies Associées, Université de Lille, and Department of Hematology, CHU Lille, Lille, France; [6]Department of Radiology, Memorial Sloan Kettering Cancer Center, New York, New York; and [7]Molecular Imaging and Therapy Service, Memorial Sloan Kettering Cancer Center, New York, New York

^{89}Zr-immuno-PET is a promising noninvasive clinical tool that measures target engagement of monoclonal antibodies (mAbs) to predict toxicity in normal tissues and efficacy in tumors. Quantification of ^{89}Zr-immuno-PET will need to move beyond SUVs, since total uptake may contain a significant non–target-specific contribution. Nonspecific uptake is reversible (e.g., blood volume) or irreversible (due to ^{89}Zr-residualization after mAb degradation). The aim of this study was to assess nonspecific uptake in normal tissues as a first critical step toward quantification of target engagement in normal tissues and tumors using ^{89}Zr-immuno-PET. **Methods:** Data from clinical studies with 4 ^{89}Zr-labeled intact IgG1 antibodies were collected, resulting in a total of 128 PET scans (1–7 d after injection from 36 patients: ^{89}Zr-obinutuzumab [n = 9], ^{89}Zr-cetuximab [n = 7], ^{89}Zr-huJ591 [n = 10], and ^{89}Zr-trastuzumab [n = 10] [denoted as ^{89}Zr-anti-CD20, ^{89}Zr-anti-EGFR, ^{89}Zr-anti-PSMA and ^{89}Zr-anti-HER2, respectively]). Nonspecific uptake was defined as uptake measured in tissues without known target expression. Patlak graphical evaluation of transfer constants was used to estimate the reversible (V_t) and irreversible (K_i) contributions to the total measured uptake for the kidney, liver, lung, and spleen. Baseline values were calculated per tissue combining all mAbs without target expression (kidney: ^{89}Zr-anti-CD20, ^{89}Zr-anti-EGFR, and ^{89}Zr-anti-HER2; liver: ^{89}Zr-anti-CD20; lung: ^{89}Zr-anti-CD20, ^{89}Zr-anti-EGFR, and ^{89}Zr-anti-PSMA; spleen: ^{89}Zr-anti-EGFR and ^{89}Zr-anti-HER2). **Results:** For the kidney, liver, lung, and spleen, baseline V_t was 0.20, 0.24, 0.09, and 0.24 mL·cm^{-3}, respectively, and baseline K_i was 0.7, 1.1, 0.2 and 0.5 μL·g^{-1}·h^{-1}, respectively. For ^{89}Zr-anti-PSMA, a 4-fold higher K_i was observed for the kidney, indicating target engagement. In this case, nonspecific uptake accounted for 66%, 34%, and 22% of the total signal in the kidney at 1, 3, and 7 d after injection, respectively. **Conclusion:** This study shows that nonspecific uptake of mAbs for tissues without target expression can be quantified using ^{89}Zr-immuno-PET at multiple time points. These results form a crucial base for measurement of target engagement by therapeutic antibodies in vivo with ^{89}Zr-immuno-PET. For future studies, a pilot phase including at least 3 scans at 1 or more days after injection is required to assess nonspecific uptake as a function of time, to optimize study design for detection of target engagement.

Key Words: immuno-PET; monoclonal antibodies; ^{89}Zr; molecular imaging; positron emission tomography

J Nucl Med 2019; 60:1825–1832
DOI: 10.2967/jnumed.118.224568

In vivo assessment of target engagement is of interest to understand efficacy (tumor selectivity) and toxicity (due to target expression in normal tissues) of treatment with monoclonal antibodies (mAbs) or mAb conjugates. Currently, only plasma concentrations of mAbs can be easily measured in vivo by obtaining blood samples. Direct measurement in tissues is difficult, as this requires invasive tissue sampling, limiting clinical application.

^{89}Zr-immuno-PET is a noninvasive, whole-body technique with the potential to measure target engagement of therapeutic antibodies (or mAb conjugates) in vivo (*1*). Future applications of this clinical tool are selection of mAbs during drug development and selection of patients who are likely to benefit from treatment (*2*).

Currently, it is common practice to report a single uptake value, expressed as SUV or percentage injected activity per milliliter, for ^{89}Zr-immuno-PET. However, the measured uptake in tissue is the sum of specific uptake (target engagement by the therapeutic antibody) and nonspecific uptake (i.e., activity in the blood vessels or in the interstitial space that does not interact with the target and therefore has no pharmacologic effects). The ratio between specific uptake and nonspecific uptake is expected to be time-dependent. Measured uptake at early time points consists mainly of the blood volume fraction, whereas specific uptake increases over time. If specific uptake dominates, a single uptake value is an appropriate estimate to assess target engagement (*3*). This measurement is then expected to correlate with target expression in biopsies (determined by immunohistochemistry) and treatment outcome. However, biopsy sampling also has several limitations,

Received Dec. 6, 2018; revision accepted Apr. 8, 2019.
For correspondence or reprints contact: Yvonne W.S. Jauw, Amsterdam UMC, De Boelelaan 1117, 1081 HV Amsterdam, The Netherlands.
E-mail: yws.jauw@vumc.nl
Published online May 30, 2019.

such as sampling error and heterogeneity in target expression. Although biopsy may not provide a true gold standard for target engagement, it is the commonly available comparator. So far, clinical ^{89}Zr-immuno-PET studies have reported equivocal results, sometimes suggesting a correlation and sometimes not (*4–7*). These results indicate that a single uptake value could be insufficient because of the contribution of nonspecific uptake. Therefore, knowledge of nonspecific uptake is required to optimize study design.

The aim of this study was to assess nonspecific uptake for tissues without target expression, as a first step toward quantification of target engagement using ^{89}Zr-immuno-PET.

Nonspecific uptake is due to the blood volume fraction of the tissue, as well as antibody distribution (entering the tissue interstitium through paracellular pores and through endothelial cells mediated by the neonatal Fc-receptor, and leaving the tissue by convective transport through lymph flow) (Fig. 1A) (*8*). At equilibrium, this physiologic component is linear with the plasma concentration (*9*) and is characterized as reversible uptake. In addition, nonspecific catabolism of antibodies occurs by pinocytosis (e.g., in endothelial cells) and subsequent lysosomal proteolytic degradation (*10,11*). After the antibody is degraded, ^{89}Zr residualizes, leading to another component of nonspecific uptake (Fig. 1B) (*11–13*). This component is proportional to the area under the plasma time–activity curve from the time of injection up to the scan time point and is characterized as irreversible uptake. For tissues without target expression, this uptake is solely due to residualization of ^{89}Zr after non–target-mediated degradation of the mAb.

These 2 components of nonspecific uptake can be quantified using graphical evaluation of transfer constants, commonly known as the Patlak linearization approach, as used for ^{18}F-FDG PET (*14*). For tissues without target expression, we expect transfer constants in agreement with known literature for nonbinding mAbs. For tissues with target expression, transfer constants would potentially differ because of target engagement (Fig. 1C) (*15*).

MATERIALS AND METHODS

Data Collection

^{89}Zr-immuno-PET scans and blood sample data were obtained for ^{89}Zr-obinutuzumab (*16*), ^{89}Zr-cetuximab (*17*), ^{89}Zr-huJ591 (*18*), and ^{89}Zr-trastuzumab (Table 1) (*19*). In the remainder of this report, the ^{89}Zr-labeled mAbs used in these studies will be denoted as ^{89}Zr-anti-CD20, ^{89}Zr-anti-EGFR, ^{89}Zr-anti-PSMA, and ^{89}Zr-anti-HER2, respectively. Data selection was based on the availability of scans at multiple time points (at least 3) for each patient, including plasma or serum activity concentrations from venous blood sampled at each scan time point.

Data were collected from Amsterdam UMC, CHU Lille, and Memorial Sloan Kettering Cancer Center. All studies were approved by an institutional review board and ethics committee. At CHU Lille and Memorial Sloan Kettering Cancer Center, PET scans were acquired on a Discovery PET/CT scanner (GE Healthcare). At Amsterdam UMC, PET scans were acquired on a Gemini TF-64 or Ingenuity TF-128 PET/CT scanner (Philips Healthcare). For all procedures, a low-dose CT scan was used for attenuation and scatter correction. Volumes of interest of the kidney, liver, lung, and spleen were manually delineated on each scan and characterized by the mean radioactivity concentration in Bq·cm^{-3}. All radioactivity concentrations were decay-corrected to the time of injection.

For each antibody, the Human Protein Atlas (*20*) was used as a reference for lack of target antigen expression in tissues of interest.

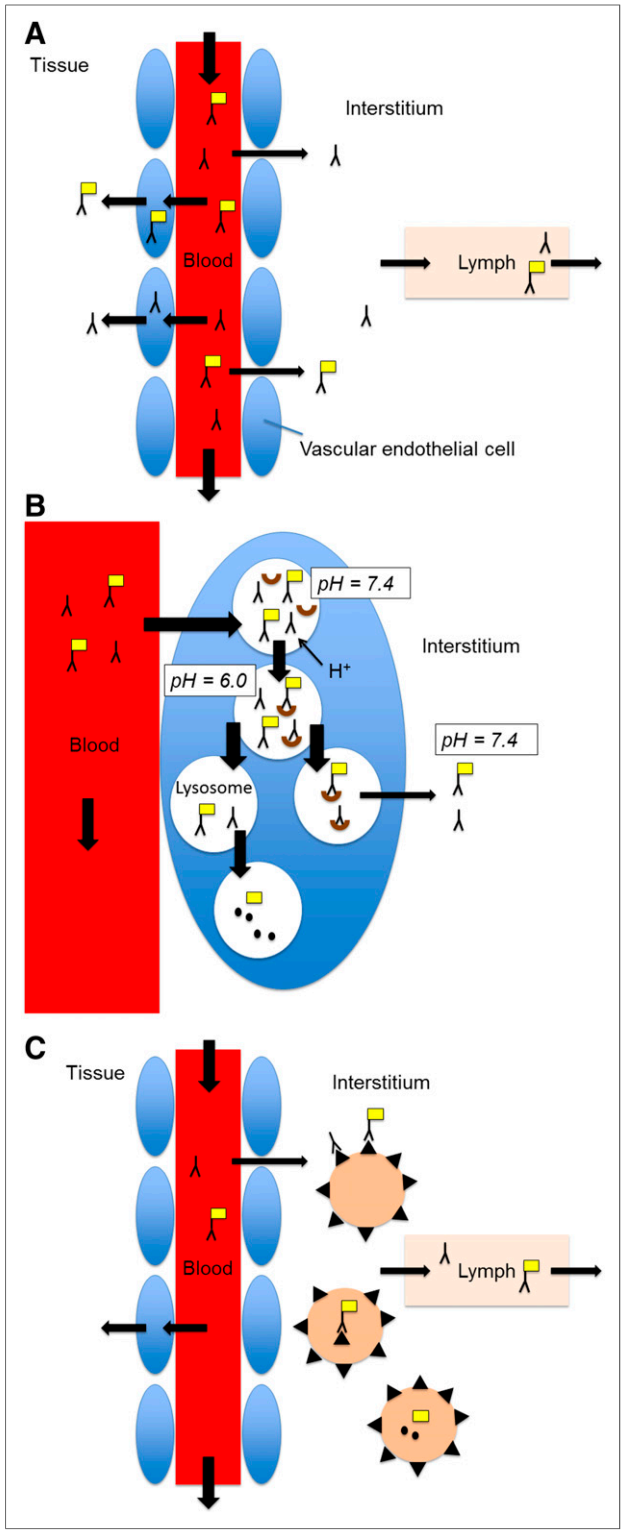

FIGURE 1. Biodistribution of ^{89}Zr-labeled mAb: physiologic components. (A) Reversible nonspecific uptake due to antibody in vascular tissue compartment and antibody entering tissue interstitium through paracellular pores, and through endothelial cells mediated by neonatal Fc-receptor, leaving tissue by convective transport through lymph flow. (B) Irreversible nonspecific uptake due to mAb degradation in lysosome, followed by residualization of ^{89}Zr. (C) Specific uptake due to target engagement (target binding and internalization of mAb-target antigen). (Adapted from Lobo et al. (*8*) and Chen et al. (*10*).)

TABLE 1
Data Characteristics

Characteristic	^{89}Zr-anti-CD20	^{89}Zr-anti-EGFR	^{89}Zr-anti-PSMA	^{89}Zr-anti-HER2
mAb	Obinutuzumab	Cetuximab	Hu-J591	Trastuzumab
Type	Humanized	Chimeric	Humanized	Humanized
IgG subclass	IgG1	IgG1	IgG1	IgG1
Target expression (*20*)				
Kidney	Absent	Absent	Present	Absent
Liver	Absent	Present	Present	Present
Lung	Absent	Absent	Absent	Present
Spleen	Present	Absent	Absent*	Absent
Center	Amsterdam UMC (n = 4); CHU Lille (n = 5)	Amsterdam UMC	Memorial Sloan Kettering Cancer Center	Memorial Sloan Kettering Cancer Center
Patient category	Non-Hodgkin lymphoma	Colorectal carcinoma	Prostate cancer	Gastric cancer
Number of patients	9	7	10	10
Injected activity/mAb dose	37 MBq/10 mg; 1,000 mg unlabeled mAb	37 MBq/10 mg; 500 mg/m^2 unlabeled mAb	185 MBq/1.7 mg; total mass of 25 mg mAb	185 MBq/3 mg; total mass of 50 mg mAb
Administration†	Predose	Predose	Coinjection	Coinjection
PET scan time points	1 h, 72 h, 144 h after injection	1 h, 72 h, 144 h after injection	2–4 h, 24 h, 48–120 h, 144–168 h after injection	4 h, 24 h, 48–96 h, 120–192 h after injection
Blood sample‡	Plasma	Plasma	Serum	Serum
Blood sampling time points	5, 30, 60, 120 min; 24¶, 72, 144 h after injection	1–2, 24, 48, 72, 144 h	5, 30, 60, 120–240 min; 24, 48–120, 144–168 h after injection	5, 15, 30, 60 min; 2, 24,48–96, 120–192 h after injection
Reference	Jauw et al. (*16*)	Menke et al. (*17*)	Pandit-Taskar et al. (*18*)	O'Donoghue et al. (*19*)

*Expression of prostate-specific membrane antigen in spleen has been reported (*24*).
†Predose = ^{89}Zr-mAb within 2 h after administration of unlabeled mAb.
‡Blood samples consisted of plasma or serum samples, assuming no practical difference between these assays for our purposes because mAb binding does not occur to coagulation factors (difference between plasma and serum).
¶Blood samples obtained at 24 h after injection at CHU Lille (n = 5); no 24-h sample obtained at Amsterdam UMC.
Coinjection = unlabeled mAb infused intravenously over 5 min followed immediately by 1 min infusion of radiolabeled mAb.

Patlak Linearization

Patlak linearization applied to multiple-time tissue activity concentration measurements allows an estimate of the reversible and irreversible contributions to measured activity. The method was initially applied to blood-to-brain transfer and considered the fate of a test solute to obtain transfer constants (*14,21*). For ^{89}Zr-immuno-PET, we used this method to determine reversible and irreversible nonspecific uptake of therapeutic antibodies. This analysis was performed per patient, for each tissue (liver, spleen, lung, and kidney).

Input data consisted of the activity concentration in plasma (AC_p in Bq·mL^{-1}) and in tissue (AC_t in Bq·cm^{-3}) as a function of time after injection. The data were plotted as

$$\frac{AC_t}{AC_p} = K_i \frac{\int_0^t AC_p(\tau)d\tau}{AC_p} + V_T,$$

with AC_t/AC_p along the y-axis and $\int AC_p(\tau)d\tau/AC_p$ along the x-axis (commonly known as a Patlak plot).

The $\int AC_p(\tau)d\tau$ term represents the area under the plasma curve from the time of injection to the time of measurement and will be referred to as $AUC_p^{0\text{-}t}$. The offset of the Patlak plot represents the distribution volume, V_T (in mL·cm^{-3}), and the slope of the Patlak plot represents the net rate of irreversible uptake, K_i (in mL·g^{-1}·min^{-1}).

Late time points (defined as ≥1 d after injection) were included in the linear fit, because an equilibrium state was assumed for these time points (*1*). Early time points (scans at 1 h after injection) were therefore not included.

The quality of the linear fit was assessed if at least 3 late time points were available. An r value more than 0.9 was considered acceptable. Linear fits with an r value of less than 0.9 were excluded from the analysis.

The reversible and irreversible contributions to the uptake of ^{89}Zr-mAb (AC^f) at each time point were calculated as

$$AC_t^r = V_T \cdot AC_p, \text{ and } AC_t^i = K_i \cdot AUC_p^{0-t},$$

with superscript r for the reversible and i for the irreversible component. In addition, the percentage difference between fitted ($AC^f = AC^r + AC^i$)

and measured tissue activity concentrations per time point was calculated as $(AC^f - AC^r)/AC^t \times 100$ (%).

Predicted Values for Transfer Constants

The transfer constants obtained were interpreted in terms of physiologic components of antibody biodistribution. A literature search was performed to obtain predicted values for these physiologic components for a nonbinding intact IgG1 mAb.

To predict the value for the reversible component for a nonbinding mAb, we used the proportionality constant between the tissue and plasma concentration, referred to as the antibody biodistribution coefficient (ABC). ABCs for various tissues were obtained by a physiologically based pharmacokinetic model of mAbs and validated with experimental data (*9*). The reported ABC for brain was 0.004 (*9*), indicating that the plasma volume fraction of 0.02 (*22*) was not included. Therefore, we defined the predicted value for V_T as the ABC plus the plasma volume fraction (within a 2-fold error margin, as reported for all ABCs). The volume fraction was calculated as the plasma volume of the tissue (in mL) divided by the total volume of the tissue (in mL). Plasma and total tissue volumes were obtained from previously published physiologic model parameters for humans (*22*). For example, for the kidney, the reported ABC was 0.137 and the plasma volume fraction 0.055 (*22*), leading to a predicted V_T of 0.19. The predicted values for V_T for liver and spleen were 0.21 and 0.25, respectively (*9,22*). The ABC for lung requires special consideration, since lung has a density of about 0.3 g/mL. Volumes of distribution are in $mL \cdot cm^{-3}$; therefore, the ABC for lung was divided by 3 to compare with V_T values derived from ^{89}Zr-immuno-PET. For lung, the predicted value for V_T was 0.10 (*9,22*).

For tissues without target expression, the entire irreversible component is due to non–target-mediated mAb degradation (and subsequent residualizing of ^{89}Zr). Endosomal mAb degradation is a nonspecific catabolic mechanism for all intact IgG molecules. Per day, 6.3% of the intravascular IgG pool is catabolized (*23*). Therefore, the whole-body catabolic rate was estimated at 7.8 $mL \cdot h^{-1}$, using a reference total plasma volume (*22*). The contribution of individual tissues (experimentally determined in mice) was 6%, 30%, 1.3%, and 2.8% for kidney, liver, lung, and spleen, respectively (*11*). These values were used to predict the irreversible component for tissues without target expression.

To compare the ^{89}Zr-immuno-PET–derived value for the net rate of irreversible uptake in $\mu L \cdot g^{-1} \cdot h^{-1}$ to the catabolic rate in $mL \cdot h^{-1}$, K_i was multiplied by tissue volume (*22*).

Predicted values for V_T and K_i, including literature values used, are presented in Supplemental Table 1 (supplemental materials are available at http://jnm.snmjournals.org).

Statistical Analysis

Values for V_T and K_i are presented per tissue and per ^{89}Zr-mAb. Median values and interquartile ranges (IQs) are reported because of the small sample size per group.

In addition, a baseline value was obtained by combining the n values for tissues without target expression. For example, no target expression in the kidney was reported for CD20, EGFR, and HER2

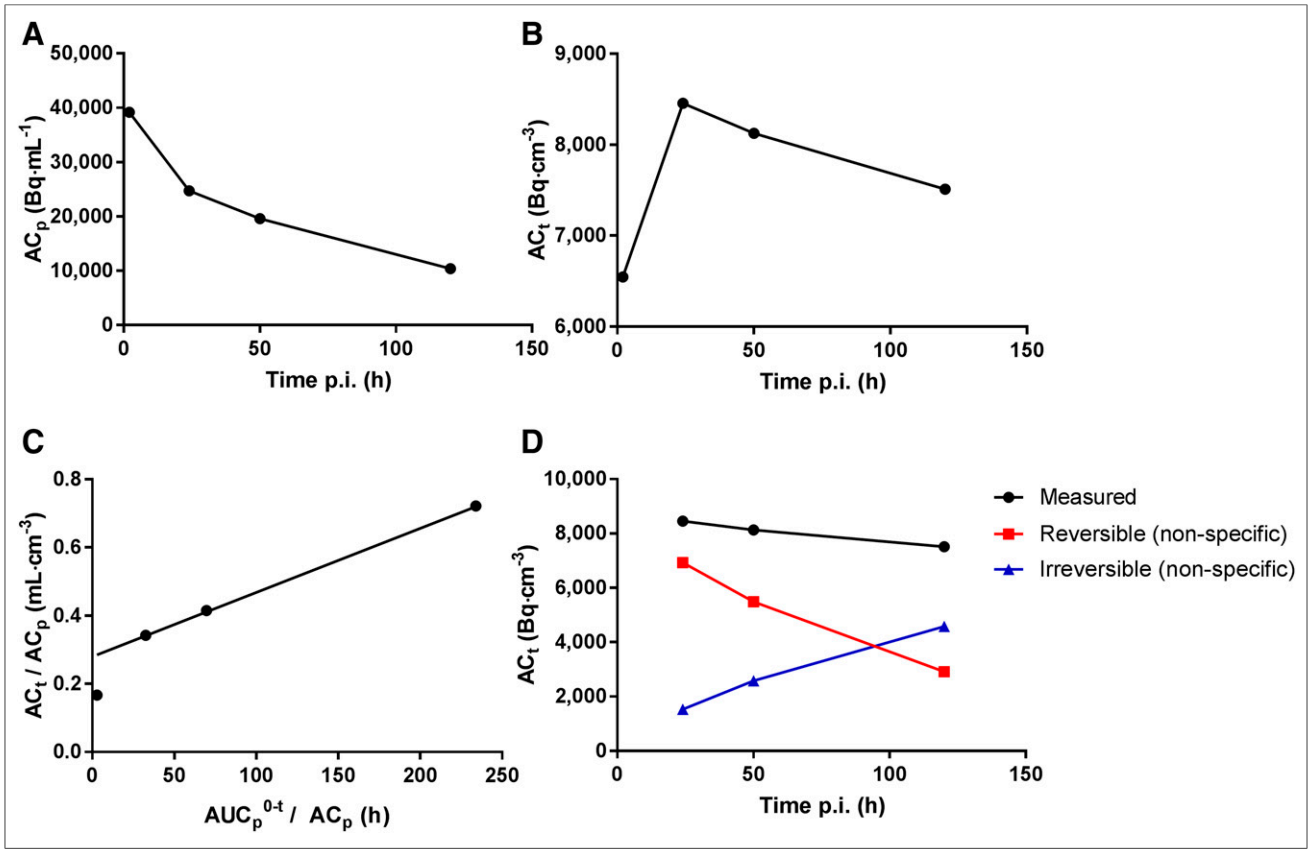

FIGURE 2. Transfer constants for ^{89}Zr-anti-HER2 in kidney. (A and B) Example for 1 patient in ^{89}Zr-anti-HER2 study, with measured activity concentrations in serum (A) and measured activity concentrations in kidney (B). (C) Patlak linearization to determine offset (V_T) and slope (K_i) of linear fit to last 3 time points (same data). (D) Reversible and irreversible contributions to total measured signal. No target expression has been reported for HER2 in normal kidney. Therefore, we hypothesize that total signal consists of nonspecific uptake. After 100 h after injection, total uptake predominantly consists of irreversible nonspecific uptake due to ^{89}Zr-residualization after mAb degradation. p.i. = after injection.

TABLE 2
V_t

Site	^{89}Zr-anti-CD20	^{89}Zr-anti-EGFR	^{89}Zr-anti-PSMA	^{89}Zr-anti-HER2	Baseline
Kidney	0.18 (0.15–020)	0.25 (0.23–0.29)	0.28 (0.21–0.32)	0.19 (0.15–0.25)	0.20 (0.16–0.25)
Liver	0.24 (0.21–0.28)	0.64 (0.54–0.91)	0.29 (0.23–0.43)	0.24 (0.22–0.29)	0.24 (0.21–0.28)
Lung	0.08 (0.08–0.10)	0.11 (0.09–0.13)	0.07 (0.06–0.09)	0.08 (0.05–0.11)	0.09 (0.07–0.10)
Spleen	0.20 (0.18–0.21)	0.23 (0.20–0.27)	0.22 (0.20–0.28)	0.24 (0.18–0.27)	0.24 (0.20–0.27)

V_t (mL·cm^{-3}) is presented as median followed by IQ in parentheses.

(Table 1) (*20*). Therefore, ^{89}Zr-anti-CD20, ^{89}Zr-anti-EGFR, and ^{89}Zr-antiHER2 data were combined to determine the baseline value for V_T and K_i for kidney tissue without target expression. Baseline values for liver consisted of ^{89}Zr-anti-CD20. For lung, data on ^{89}Zr-anti-CD20, ^{89}Zr-anti-EGFR, and ^{89}Zr-anti-PSMA were combined to obtain the baseline value. For spleen, the baseline value consisted of ^{89}Zr-anti-EGFR and ^{89}Zr-anti-HER2.

The Wilcoxon signed-rank test was used to determine whether the n values for V_T for tissues without target expression (baseline values) differed from the predicted value. A P value of less than 0.05 was considered statistically significant. Statistical tests were performed in GraphPad Prism, version 6.02.

RESULTS

Patlak Linearization

Per patient, Patlak linearization was conducted for each tissue (kidney, liver, lung, and spleen) (Fig. 2). An r value of more than 0.9 was obtained for 71 of 80 linear fits for ^{89}Zr-anti-PSMA and ^{89}Zr-anti-HER2 (3 late time points available). Therefore, we assumed that data for ^{89}Zr-anti-CD20 and ^{89}Zr-EGFR were consistent with the assumptions under the Patlak method. For these datasets, the r value for the linear fit could not be obtained (only 2 late time points available). For ^{89}Zr-anti-HER2, an r value of less than 0.9 was obtained for 1 of 10 fits for kidney uptake, 2 of 10 for liver, 4 of 10 for lung, and 2 of 10 for spleen. The mean percentage difference between fitted and measured tissue activity concentrations per time point for all fits through 3 time points with an r value of more than 0.9 was ±4%, except for ^{89}Zr-anti-PSMA in the kidney (Supplemental Table 2).

V_T

Values for V_T per mAb are presented in Table 2. Nonspecific, reversible uptake is reflected by baseline values for V_T for tissues without target expression. For the kidney, liver, lung, and spleen, respectively, measured median baseline values for V_T were 0.20 (IQ, 0.16–0.25), 0.24 (IQ, 0.21–0.28), 0.09 (IQ, 0.07–0.10), and 0.24 (IQ, 0.20–0.27) mL·cm^{-3}. For these tissues, the predicted values for V_T (ABC + plasma volume fraction) were 0.19, 0.21, 0.10, and 0.25, respectively. No differences were observed between the measured baseline value for V_T and the predicted value for kidney ($P = 0.24$; $n = 25$), liver ($P = 0.07$; $n = 9$), and spleen ($P = 0.12$; $n = 15$). For lung, the measured baseline value for V_T (0.09, 0.07–0.10) was statistically different ($P < 0.02$; $n = 25$) from the predicted value of 0.10 but within the 2-fold error range (0.05–0.20) of the predicted value.

K_i

Values for K_i per mAb are presented in Table 3. Nonspecific, irreversible uptake is reflected by baseline values for K_i for tissues without target expression. For kidney, liver, lung, and spleen, respectively, measured baseline values for K_i were 0.7 (IQ, 0.4–1.3), 1.1 (IQ, 0.8–2.1), 0.2 (IQ, 0.1–0.3), and 0.5 (IQ, 0.3–0.7) μL·g^{-1}·h^{-1}. For kidney, the baseline catabolic rate was 0.23 mL·h^{-1}, equal to 3% of the whole-body catabolic rate (predicted value, 6%). Fractional catabolic rates of liver, lung, and spleen were 30%, 3%, and 1%, respectively (predicted values were 30%, 1.3%, and 2.8%).

Detection of Target Engagement

In cases of target engagement (Fig. 1C), we expect to observe an increased rate of irreversible uptake compared with the baseline value. Expression of PSMA was reported for the kidney (*18*), and target engagement of ^{89}Zr-anti-PSMA is therefore expected in this tissue. Patlak linearization for ^{89}Zr-anti-PSMA was performed (Fig. 3). In this case, a 4-fold increased K_i (2.8 vs. 0.7) was obtained compared with the baseline value for the kidney, indicating target engagement by irreversible uptake. For liver, an increased K_i was observed for ^{89}Zr-anti-EGFR, ^{89}Zr-anti-PSMA,

TABLE 3
K_i

Site	^{89}Zr-anti-CD20	^{89}Zr-anti-EGFR	^{89}Zr-anti-PSMA	^{89}Zr-anti-HER2	Baseline
Kidney	0.4 (0.2–0.6)	0.7 (0.4–1.2)	2.8 (2.4–3.1)	1.5 (0.9–1.8)	0.7 (0.4–1.3)
Liver	1.1 (0.8–2.1)	3.8 (1.9–5.8)	5.7 (4.9–8.4)	1.7 (1.4–2.0)	1.1 (0.8–2.1)
Lung	0.2 (0.1–0.3)	0.4 (0.2–0.6)	0.1 (0.0–0.2)	0.2 (0.0–0.5)	0.2 (0.1–0.3)
Spleen	0.6 (0.5–0.8)	0.5 (0.3–0.5)	1.5 (1.2–1.7)	0.7 (0.4–0.8)	0.5 (0.3–0.7)

K_i (μL·g^{-1}·h^{-1}) is presented as median followed by IQ in parentheses.

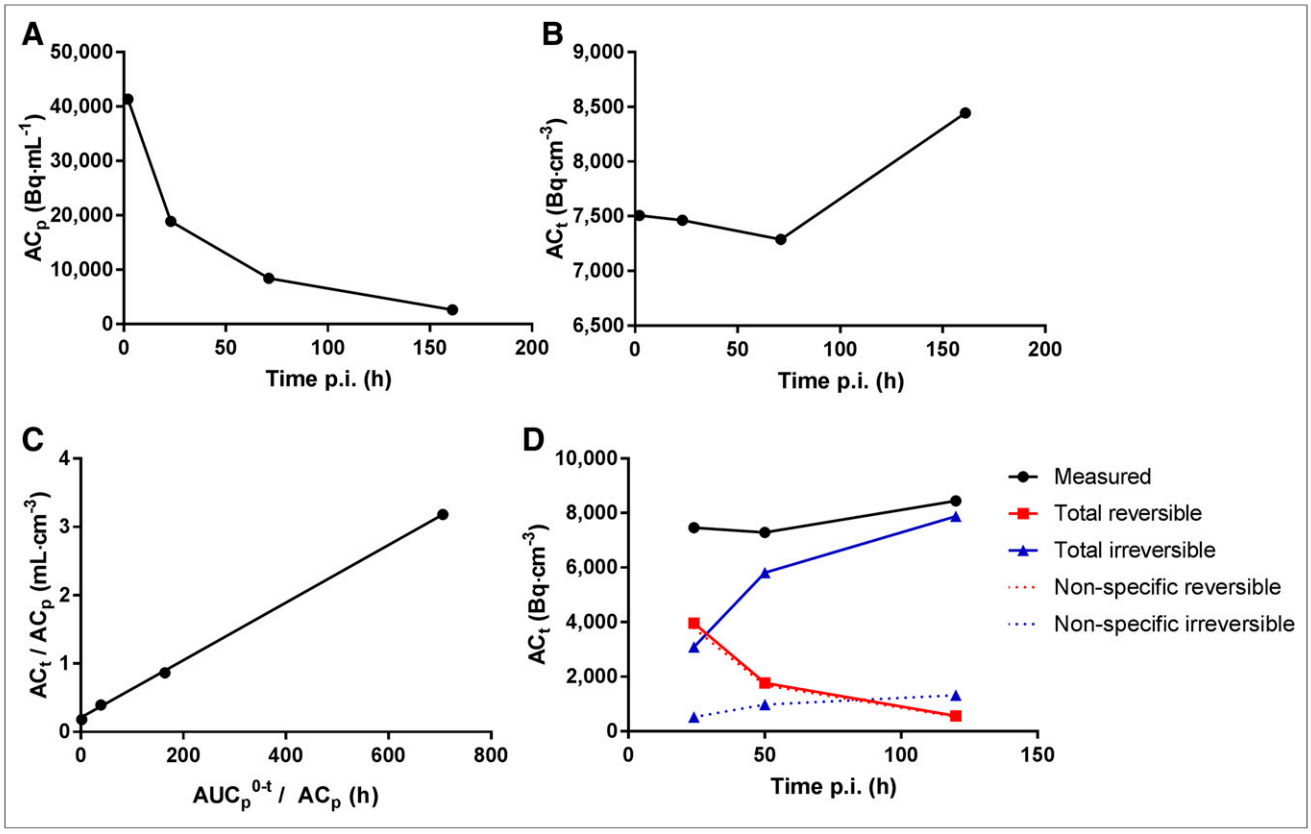

FIGURE 3. Transfer constants for ^{89}Zr-anti-PSMA in kidney. (A and B) Example for 1 patient in ^{89}Zr-anti-PSMA study, with measured activity concentrations in serum (A) and measured activity concentrations in kidney (B). (C) Patlak linearization to determine offset (V_T) and slope (K_i) of linear fit to last 3 time points (same data). (D) Total reversible and total irreversible contributions to measured signal. Dashed lines represent estimated values for nonspecific reversible uptake (calculated as baseline $V_T \cdot AC_p$) and nonspecific irreversible uptake (calculated as baseline $K_i \cdot AUC_p^{0-t}$). Nonspecific uptake accounts for 66%, 34%, and 22% of total measured signal at 1, 3, and 7 d after injection, respectively. Difference between total irreversible uptake and estimated nonspecific irreversible uptake indicates target-mediated uptake. p.i. = after injection.

and ^{89}Zr-anti-HER2 (3.8, 5.7, and 1.7, respectively, compared with 1.1), corresponding to known target expression (*20*). No increased K_i was observed for lung or spleen (Table 3).

DISCUSSION

^{89}Zr-immuno-PET is a promising noninvasive clinical tool to measure antibody target engagement in vivo. As a first step toward quantification of target engagement, nonspecific uptake for tissues without target expression was assessed for 4 ^{89}Zr-labeled mAbs. This study showed that nonspecific, reversible uptake (V_T) was similar to the predicted value for a nonbinding mAb. Nonspecific, irreversible uptake (K_i) corresponded to the predicted value for the fractional catabolic rate of IgG. Patlak linearization is applied to data obtained from a single subject. The range of values observed for the baseline transfer constants reflects interpatient variability. This method allows, for a single subject, assessment of whether target-mediated binding does occur in a certain normal tissue for the antibody under investigation. Similar to the pharmacokinetic–pharmacodynamic type of analysis, Patlak linearization can be applied with sparse temporal sampling but does not require assumptions that underlying parameters are the same among patients. Moreover, it uses the individually measured input functions, that is, bioavailability of the tracer in blood over time, and it can therefore account for interindividual variability of the tracer bioavailability in the central compartment (i.e., blood). For these reasons, this method was applied in our present study. An increase in K_i indicates target engagement, as was observed for, for example, ^{89}Zr-anti-PSMA in the kidney. In this study, baseline values for K_i and V_T were tissue-dependent. Especially for the liver, relatively high nonspecific, irreversible uptake was observed compared with other tissues, indicating that this organ is strongly involved in mAb catabolism. Therefore, detection of target engagement with a single uptake value is expected to be more difficult in the liver.

Study design can have a significant impact on the ability to detect target engagement. For example, for ^{89}Zr-anti-CD20, no increase of irreversible uptake (K_i) was observed in the spleen, although expression of CD20 in the spleen is known to be high (*20*). A plausible explanation for this observation is saturation of the CD20 receptors due to a high dose of unlabeled anti-CD20 (1,000 mg), which was administered before the radiolabeled antibody. So, antibody dose is a parameter to be considered in assessment of target engagement. Another important consideration for design of ^{89}Zr-immuno-PET studies is that scans obtained at multiple late time points are required for the Patlak linearization to determine reversible and irreversible uptake. At least 3 late time points are required to assess whether the data can be fitted to a straight line.

In some cases (9/80), the data could not be described by a linear fit. Especially for the lung (4/9), this finding could be explained by an unfavorable signal-to-noise ratio (low signal and relatively low tissue density). The observed overestimation of fitted uptake data at 24 h after injection accompanied by an underestimation of the uptake at 48–120 h after injection for ^{89}Zr-anti-PSMA in the kidney only may indicate that the reversible uptake processes were not yet in the equilibrium state at 24 h after injection. From a methodologic perspective, collection of more data points would be preferred. This method could be further validated in future preclinical ^{89}Zr-immuno-PET studies in which scans at more time points are acquired, including invasive tissue sampling to assess target expression by immunohistochemistry.

Usually, ^{89}Zr-immuno-PET scans are analyzed at a single time point, representing the sum of all physiologic components of antibody distribution, being either target-specific or nonspecific. This study showed how the various physiologic components of antibody distribution contribute to the measured SUV (Figs. 2 and 3). For the kidney, as an example, an SUV of around 2.5 was measured for ^{89}Zr-anti-PSMA at 1–7 d after injection. Nonspecific uptake was estimated to account for an SUV of 1.6 (66%) at 1 d after injection. The contribution of nonspecific uptake decreased to an SUV of 0.6 (22%) at 7 d after injection.

Detection of target engagement in normal tissues is of interest to assess which mAb has potential for further development into an antibody–drug conjugate (ADC). For an ADC, absence of target engagement in normal tissues is considered important to limit potential toxicity.

To understand and predict the efficacy of mAb-based treatments, measurement of target engagement in tumors is essential. However, the method described in this paper cannot be directly applied to tumors, as these are expected to be more complex than normal tissues. Nonspecific, reversible uptake in tumors (blood volume fraction and non–target-mediated antibody distribution to tumor tissue ["tight" or "leaky" tissue]) may be more variable between tumors and between patients. In addition, nonspecific, irreversible uptake may be increased by the rate of protein catabolism in the tumor and uptake in tumor immune filtrates (e.g., macrophages). In future work, we aim to explore which method can be applied to measure target engagement for tumors. Especially target-negative tumors are of interest to study factors that influence nonspecific uptake.

In the present study, ^{89}Zr-immuno-PET was used as a noninvasive clinical tool to assess physiologic components of antibody distribution in vivo, and target engagement of therapeutic antibodies was observed. For future studies to assess target engagement for other ^{89}Zr-labeled mAbs, a multiple time point pilot study (with at least 3 late time points) is advised to determine the contribution of nonspecific uptake as a function of time and mAb dose. This knowledge can be used to optimize study design and assess whether single time point scanning to detect target engagement is feasible and at which time point.

This concept is widely applicable because mAbs and mAb conjugates against many target antigens are developed for a broad range of clinical indications.

CONCLUSION

This study shows that nonspecific uptake of mAbs for tissues without target expression can be quantified using ^{89}Zr-immuno-PET at multiple time points. These results form a crucial base for measurement of target engagement by therapeutic antibodies in vivo with ^{89}Zr-immuno-PET. For future studies, a pilot phase including at least 3 scans at 1 or more days after injection is required to assess nonspecific uptake as a function of time and optimize study design for detection of target engagement.

DISCLOSURE

This research was financially supported by the Dutch Cancer Society (grant VU2013-5839 to Yvonne Jauw) and the Cancer Center Amsterdam (travel grant to Yvonne Jauw). Wolfgang Weber received research support from Ipsen, Piramal, BMS, and Blue Earth Diagnostics and is an advisor to Advanced Accelerator Applications, Bayer, Blue Earth Diagnostics, Ipsen, Endocyte, Piramal, and Progenics. No other potential conflict of interest relevant to this article was reported.

ACKNOWLEDGMENT

We thank Mats Bergstrom (independent external imaging consultant, Uppsala, Sweden) for conceptual support.

KEY POINTS

QUESTION: Can we move quantification of ^{89}Zr-immuno-PET beyond SUV, since total uptake may contain a significant non–target-specific contribution?

PERTINENT FINDINGS: In this retrospective analysis of clinical ^{89}Zr-immuno-PET studies, nonspecific uptake was quantified in normal tissues without target expression. The magnitude of nonspecific uptake in normal tissues was related to its physiologic basis (i.e., blood volume, mAb biodistribution, and ^{89}Zr-residualization after mAb degradation).

IMPLICATIONS FOR PATIENT CARE: Nonspecific uptake of ^{89}Zr-labeled mAbs in normal tissues can be quantified to optimize detection of target engagement of therapeutic antibodies in vivo.

REFERENCES

1. Bergstrom M. The use of microdosing in the development of small organic and protein therapeutics. *J Nucl Med.* 2017;58:1188–1195.
2. Jauw YWS, Menke-van der Houven van Oordt CW, Hoekstra OS, et al. Immuno-positron emission tomography with zirconium-89-labeled monoclonal antibodies in oncology: what can we learn from initial clinical trials? *Front Pharmacol.* 2016;7:131.
3. Lammertsma AA. Forward to the past: the case for quantitative PET imaging. *J Nucl Med.* 2017;58:1019–1024.
4. Gaykema SB, Brouwers AH, Lub-de Hooge MN, et al. ^{89}Zr-bevacizumab PET imaging in primary breast cancer. *J Nucl Med.* 2013;54:1014–1018.
5. Lamberts TE, Menke-van der Houven van Oordt CW, Ter Weele EJ, et al. ImmunoPET with anti-mesothelin antibody in patients with pancreatic and ovarian cancer before anti-mesothelin antibody-drug conjugate treatment. *Clin Cancer Res.* 2016;22:1642–1652.
6. Jauw YW, Zijlstra JM, de Jong D, et al. Performance of ^{89}Zr-labeled-rituximab-PET as an imaging biomarker to assess CD20 targeting: a pilot study in patients with relapsed/refractory diffuse large B cell lymphoma. *PLoS One.* 2017;12:e0169828.
7. McKnight BN, Viola-Villegas NT. ^{89}Zr-immunoPET companion diagnostics and their impact in clinical drug development. *J Labelled Comp Radiopharm.* 2018;61:727–738.
8. Lobo ED, Hansen RJ, Balthasar JP. Antibody pharmacokinetics and pharmacodynamics. *J Pharm Sci.* 2004;93:2645–2668.
9. Shah DK, Betts AM. Antibody biodistribution coefficients: inferring tissue concentrations of monoclonal antibodies based on the plasma concentrations in several preclinical species and human. *MAbs.* 2013;5:297–305.

10. Chen Y, Balthasar JP. Evaluation of a catenary PBPK model for predicting the in vivo disposition of mAbs engineered for high-affinity binding to FcRn. *AAPS J.* 2012;14:850–859.
11. Eigenmann MJ, Fronton L, Grimm HP, et al. Quantification of IgG monoclonal antibody clearance in tissues. *MAbs.* 2017;9:1007–1015.
12. Cheal SM, Punzalan B, Doran MG, et al. Pairwise comparison of ^{89}Zr- and ^{124}I-labeled cG250 based on positron emission tomography imaging and nonlinear immunokinetic modeling: in vivo carbonic anhydrase IX receptor binding and internalization in mouse xenografts of clear-cell renal cell carcinoma. *Eur J Nucl Med Mol Imaging.* 2014;41:985–994.
13. Ferl GZ, Kenanova V, Wu AM, DiStefano JJ. A two-tiered physiologically based model for dually labeled single-chain Fv-Fc antibody fragments. *Mol Cancer Ther.* 2006;5:1550–1558.
14. Patlak CS, Blasberg RG, Fenstermacher JD. Graphical evaluation of blood-to-brain transfer constants form multiple-time uptake data. *J Cereb Blood Flow Metab.* 1983;3:1–7.
15. Li Z, Krippendorff BF, Sharma S, et al. Influence of molecular size on tissue distribution of antibody fragments. *MAbs.* 2016;8:113–119.
16. Jauw Y, Zijlstra J, Hoekstra O, et al. First-in-human in-vivo biodistribution of a glyco-engineered antibody: ^{89}Zirconium-labeled obinutuzumab in patients with non-Hodgkin lymphoma [abstract]. *J Nucl Med.* 2017;58(suppl 1): 387.
17. Menke-van der Houven van Oordt CW, Gootjes EC, Huisman MC, et al. ^{89}Zr-cetuximab PET imaging in patients with advanced colorectal cancer. *Oncotarget.* 2015;6:30384–30393.
18. Pandit-Taskar N, O'Donoghue JA, Beylergil V, et al. ^{89}Zr-huJ591 immuno-PET imaging in patients with advanced metastatic prostate cancer. *Eur J Nucl Med Mol Imaging.* 2014;41:2093–2105.
19. O'Donoghue JA, Lewis JS, Pandit-Taskar N, et al. Pharmacokinetics, biodistribution, and radiation dosimetry for ^{89}Zr-trastuzumab in patients with esophagogastric cancer. *J Nucl Med.* 2018;59:161–166.
20. Uhlen M, Oksvold P, Fagerberg L, et al. Towards a knowledge-based Human Protein Atlas. *Nat Biotechnol.* 2010;28:1248–1250.
21. Blasberg RG, Fenstermacher JD, Patlak CS. Transport of α-aminoisobutyric acid across brain capillary and cellular membranes. *J Cereb Blood Flow Metab.* 1983; 3:8–32.
22. Shah DK, Betts AM. Towards a platform PBPK model to characterize the plasma and tissue disposition of monoclonal antibodies in preclinical species and human. *J Pharmacokinet Pharmacodyn.* 2012;39:67–86.
23. Waldmann TA, Strober W. Metabolism of immunoglobulins. *Prog Allergy.* 1969;13: 1–110.
24. Weineisen M, Schottelius M, Simecek J. ^{68}Ga- and ^{177}Lu-labeled PSMA I&T: optimization of a PSMA-targeted theranostic concept and first proof-of-concept human studies. *J Nucl Med.* 2015;56:1169–1176.